Article

Metabolic Regio- and Stereoselectivity of Cytochrome P450 2D6 towards 3,4-Methylenedioxy-*N*-alkylamphetamines: in Silico Predictions and Experimental Validation

Peter H. J. Keizers, Chris de Graaf, Frans J. J. de Kanter, Chris Oostenbrink, K. Anton Feenstra, Jan N. M. Commandeur, and Nico P. E. Vermeulen

J. Med. Chem., **2005**, 48 (19), 6117-6127• DOI: 10.1021/jm050338+ • Publication Date (Web): 19 August 2005

Metabolic Regio- and Stereoselectivity of Cytochrome P450 2D6 towards 3,4-Methylenedioxy-*N*-alkylamphetamines: in Silico Predictions and Experimental Validation

Peter H. J. Keizers,[†,‡] Chris de Graaf,[†,‡] Frans J. J. de Kanter,[§] Chris Oostenbrink,[‡] K. Anton Feenstra,[‡] Jan N. M. Commandeur,[‡] and Nico P. E. Vermeulen*[,‡]

Leiden Amsterdam Center for Drug Research (LACDR)/Division of Molecular Toxicology and Division of Organic and Inorganic Chemistry, Department of Chemistry and Pharmacochemistry, Vrije Universiteit, De Boelelaan 1083, 1081 HV Amsterdam, The Netherlands

Received April 12, 2005

A series of 3,4-methylenedioxy-*N*-alkylamphetamines (MDAAs) were automatically docked and subjected to molecular dynamics (MD) simulations in a cytochrome P450 2D6 (CYP2D6) protein model. The predicted substrate binding orientations, sites of oxidation, and relative reactivities were compared to the experimental data of wild-type and Phe[120]Ala mutant CYP2D6. Automated docking results were not sufficient to accurately rationalize experimental binding orientations of 3,4-methylenedioxy-*N*-methylamphetamine (MDMA) in the two enzymes as measured with spin lattice relaxation NMR. Nevertheless, the docking results could be used as starting structures for MD simulations. Predicted binding orientations of MDMA and sites of oxidation of the MDAAs derived from MD simulations matched well with the experimental data. It appeared the experimental results were best described in MD simulations considering the nitrogen atoms of the MDAAs in neutral form. Differences in regioselectivity and stereoselectivity in the oxidative metabolism of the MDAAs by the Phe[120]Ala mutant CYP2D6 were correctly predicted, and the effects of the Phe[120]Ala mutation could be rationalized as well.

Introduction

Cytochromes P450 (CYPs) are heme containing enzymes which can be found in virtually all organisms. This large family of enzymes is capable of oxidizing and reducing a broad range of endogenous and exogenous substrates, such as steroids, carcinogens, and drugs.[1,2] In humans, one of the most relevant drug metabolizing CYPs is CYP2D6. Although the expression levels of CYP2D6 are only 2% of all hepatic CYPs, following CYP3A4, it is the second most important drug metabolizing enzyme, involved in the metabolism of about 30% of the currently marketed drugs, including β-blockers, neuroleptics, antidepressants, and antiarythmics.[3−5] Large interindividual differences exist in CYP2D6 activity, due to gene multiplicity and polymorphisms, thus further increasing its clinical importance.[6,7] The rationalization and prediction of potential CYP2D6 substrates is, therefore, advantageous in the discovery and development of new drugs. Nowadays, the first crystal structures of mammalian CYPs are becoming available.[8−10] However, so far, a crystal structure of CYP2D6 remains to be resolved, and any structural information on this enzyme still depends on homology modeling, mutagenesis, and spectroscopic studies.

CYP2D6 is one of the CYP isoforms studied most extensively using molecular modeling.[11] Several homology model structures of CYP2D6 have been built, refined, and validated experimentally. The homology models of CYP2D6 suggest that substrates interact with two or three aromatic/hydrophobic residues, e.g., Phe[120] and Phe[483], and a carboxylic acid residue, Glu[216] or Asp[301].[12,13] The relevance of these residues was supported by site-directed mutagenesis studies,[14−18] and these interactions are consistent as well with those derived from pharmacophore models of inhibitors and substrates.[19,20] Molecular modeling can provide information on active site characteristics and the importance of specific amino acid residues in enzyme−substrate interactions, but it can also be used to rationalize and predict regio- and stereoselectivity in metabolism by CYPs. It has recently also been shown that automated docking can successfully be applied to predict sites of oxidation in substrates using CYP crystal structures.[21] Molecular dynamics (MD) simulations in addition can account for distributions of multiple binding conformations and, thus, give a more comprehensive description of multiple sites of oxidation in substrates catalyzed by CYPs.[22−25]

In this study, a molecular modeling approach has been used to study the binding orientation and the sites of oxidation of a series of 3,4-methylenedioxy-*N*-alkylamphetamines (MDAAs), or XTC analogues, by CYP2D6. The primary aim was to evaluate an integrated molecular modeling approach to rationalize and predict substrate binding and metabolism by CYP2D6. When regioselectivity and stereoselectivity in drug metabolism and the effect of active site mutations can be rationalized for a series of closely related compounds, such an approach can be considered to be accurate and reliable.

* Author for correspondence: e-mail npe.vermeulen@few.vu.nl; phone 0031 20 5987590; fax 0031 20 5987610.
† Both authors contributed equally.
‡ Division of Molecular Toxicology.
§ Division of Organic and Inorganic Chemistry.

10.1021/jm050338+ CCC: $30.25
Published on Web 08/19/2005

The molecular modeling predictions were based on a homology model of CYP2D6. Reactive substrate poses were generated using automated docking and were obtained from MD simulations of wild-type and mutant CYP2D6 protein containing all three MDAAs. Two different protonation states of the basic nitrogen atom were studied, as it is known that this can drastically influence the oxidation by CYP2D6.[26] The computational predictions were validated experimentally. The effects of mutating Phe[120] into alanine on the binding modes and metabolic products were studied for five MDAAs, i.e., 3,4-methylenedioxy-*N*-methylamphetamine (MDMA), its stereoisomers, 3,4-methylenedioxy-*N*-ethylamphetamine (MDEA), and 3,4-methylenedioxy-*N*-propylamphetamine (MDPA). For the recently described Phe[120]Ala mutant, large effects on the regioselective oxidation of MDMA were demonstrated.[18] Dissociation constants for the three MDAAs were determined by spectral titration. The metabolic products were analyzed, and furthermore, the binding orientations of MDMA in the wild-type and mutant active sites were explored experimentally by NMR spin lattice relaxation rate measurements, a technique previously used to determine hydrogen atom to heme distances in CYPs.[27−30]

Results

Expression and Purification of Wild-Type and Phe[120]Ala Mutant CYP2D6. The expression levels of both wild-type and Phe[120]Ala mutant CYP2D6 were similar as described previously.[18] The enzymes which contained a C-terminal 6 × histidine tag were purified using Ni-NTA-agarose. Eluting the enzymes from the Ni-NTA-agarose using imidazole led to a large amount of enzyme in the high spin state, and even after overnight dialysis, high spin remained the predominant state. Therefore, 0.2 mM L-histidine was preferred as eluting agent over imidazole, because it did not cause a change in spin state after dialysis yielding pure enzymes which were stable for at least 4 h at 24 °C in the presence of 5% glycerol and 100 μM of substrate, as assessed by CO-difference spectroscopy. Hardly any P420 (i.e. inactive CYP detected as an absorbance maximum at 420 nm in the CO-difference spectrum) was present in the batches of purified enzyme.

Spectral Titration of Substrates to the Enzymes. The addition of all MDAAs to purified wild-type or Phe[120]Ala mutant CYP2D6 led to a type I change in the visible absorbance spectrum. By titration of the compounds to the solutions of enzyme, the spectral dissociation constants, K_s, could be estimated (using eq 1, data shown in Table 1). While there were minor differences in affinity between the wild-type and the mutant, for both enzymes, a slightly lower K_s was found for MDEA and MDPA than for MDMA. The enantiomers of MDMA had about equal affinity for the wild-type, but a slight preference toward *S*-MDMA was observed for the mutant enzyme.

Metabolism of MDAAs. As reported previously,[18] MDMA is oxidized by the Phe[120]Ala mutant to MDA and *N*-OH-MDMA, in addition to 3,4-OH-MA, the only product formed by the wild-type enzyme (Figure 1). Elongation of the *N*-methyl chain to an ethyl or propyl yielded the corresponding products after incubation with both enzymes. MDEA was O-demethylenated by wild-type and mutant CYP2D6, and additionally, the mutant N-dealkylated and N-hydroxylated MDEA. A fourth oxidation product of MDEA by the mutant was detected at a t_R of 18.5 min, with a *m/z* of 222, fragmenting to *m/z* = 163. This product could be the aldehyde or keto form of ω- or ω-1-hydroxylation, respectively.

MDPA was O-demethylenated by wild-type and the mutant CYP2D6; the latter enzyme also N-dealkylated and N-hydroxylated this substrate. A peak with a *m/z* of 254 was found at 19.2 min with the mutant, indicating a double hydroxylation. No fragmentation took place, so the positions of the hydroxyl groups remain unknown.

Product formation from all substrates was linear for at least 10 min for both enzymes under the conditions used, so the kinetic parameters were determined for the major products (Table 2). The overall rate of oxidation by the Phe[120]Ala mutant was higher than that of wild-type CYP2D6 for all MDAAs. The rates for O-demethylenation were two to five times higher for the mutant, and the fact that more products are formed indicates an even higher increase in oxidation rates. To quantify the turnover rates, a synthetic reference compound was only available for MDA; for the other products, turnover rates were only compared in relative terms. Because the fluorescence peak areas of equal concentrations of MDA, MDMA, MDEA, and MDPA are equal, it is likely that the *N*-alkyl chain has no influence

Table 1. Estimated Dissociation Constants, K_s, (μM) of the Substrates for Wild-Type and Phe[120]Ala Mutant CYP2D6[a]

substrate	K_s, wild-type	K_s, Phe[120]Ala
R/*S*-MDMA	28 ± 3	28 ± 2
R-MDMA	43 ± 6	53 ± 2
S-MDMA	40 ± 5	38 ± 4
MDEA	19 ± 2	15 ± 4
MDPA	18 ± 1	12 ± 2

[a] All values are the means ± standard deviation (SD) of at least two independent experiments, as described in the Materials and Methods section. *R*/*S*-MDMA refers to the racemic mixture of 3,4-methylenedioxy-*N*-methylamphetamine (MDMA), and *R*-MDMA and *S*-MDMA refer to the pure *R*- and *S*-isomers of MDMA, respectively. For the corresponding *N*-ethyl- and *N*-propylamphetamines (MDEA and MDPA), racemic mixtures were used.

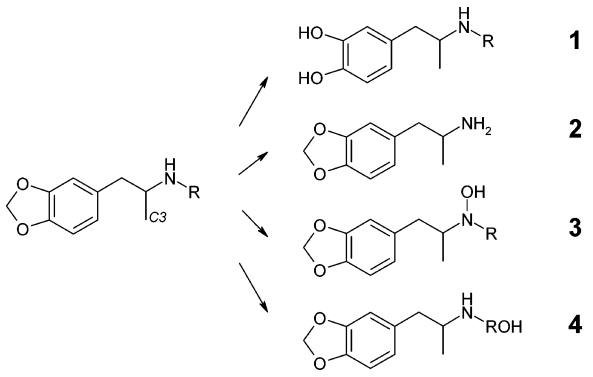

Figure 1. Scheme of the oxidation of 3,4-methylenedioxy-*N*-alkylamphetamines (MDAAs) by Phe[120]Ala mutant CYP2D6. The MDAAs are O-demethylenated to 3,4,-dihydroxy-*N*-alkylamphetamine (**1**), N-dealkylated to 3,4-methylenedioxyamphetamine (**2**), N-hydroxylated to 3,4-methylenedioxy-*N*-hydroxy-*N*-alkylamphetamine (**3**), or ω/ω-1-hydroxylated to 3,4-methylenedioxy-ω/ω-1-hydroxy-*N*-alkylamphetamine (**4**). The C_3-methyl is indicated, and R is methyl, ethyl, and propyl for MDMA, MDEA, and MDPA, respectively.

Table 2. Product Formation of the Oxidation of MDAAs by Wild-Type and Phe[120]Ala Mutant CYP2D6[d]

			wild-type		Phe[120]Ala	
substrate	product	structure	K_m	V_{max}[a]	K_m	V_{max}
R/*S*-MDMA	3,4-OH-MA	**1**	1.9 ± 0.5	1.2 ± 0.4	11.8 ± 3.8	2.2 ± 0.0[a]
	MDA	**2**	*c*	*c*	14.5 ± 2.4	3.5 ± 0.1[b]
	N-OH-MDMA	**3**	*c*	*c*	11.2 ± 1.4	7.1 ± 0.5[a]
R-MDMA	3,4-OH-MA	**1**	2.7 ± 0.4	1.2 ±0.2	13.2 ± 0.6	2.4 ± 0.1[a]
	MDA	**2**	*c*	*c*	26.1 ± 3.3	5.9 ± 0.7[b]
	N-OH-MDMA	**3**	*c*	*c*	20.6 ± 2.5	10.7 ± 1.3[a]
S-MDMA	3,4-OH-MA	**1**	3.3 ± 0.5	1.2 ± 0.0	4.9 ± 0.1	2.4 ± 0.0[a]
	MDA	**2**	*c*	*c*	10.3 ± 0.6	3.8 ± 0.1[b]
	N-OH-MDMA	**3**	*c*	*c*	6.9 ± 0.6	8.4 ± 0.4[a]
MDEA	3,4-OH-EA	**1**	1.1 ± 0.1	1.2 ± 0.2	3.3 ± 0.0	2.9 ± 0.2[a]
	MDA	**2**	*c*	*c*	4.5 ± 0.8	4.2 ± 0.1[b]
	N-OH-MDEA	**3**	*c*	*c*	5.7 ± 0.3	1.4 ± 0.1[a]
MDPA	3,4-OH-PA	**1**	1.0 ± 0.1	1.3 ± 0.1	5.2 ± 0.6	7.5 ± 0.6[a]
	MDA	**2**	*c*	*c*	9.1 ± 0.5	7.3 ± 1.8[b]
	N-OH-MDPA	**3**	*c*	*c*	28.0 ± 6.5	3.0 ± 0.2[a]

[a] V_{max} expressed in 1×10^5 fluorescence units min^{-1} $nmol^{-1}$ CYP. [b] V_{max} expressed in min^{-1}. [c] Not observed. [d] All values are the means of at least two independent experiments ± SD, as described in the Materials and Methods section. Structure numbers refer to products drawn in Figure 1; K_m is expressed in μM.

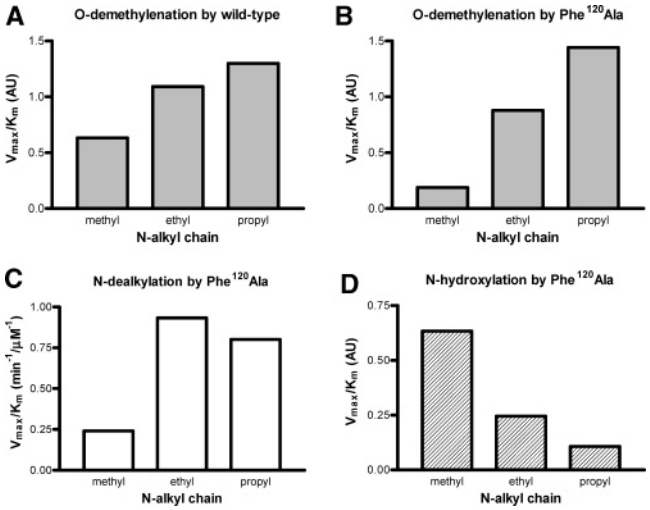

Figure 2. V_{max}/K_m product ratios (min^{-1} μM^{-1} for N-dealkylation, AU for the other products) for the O-demethylenation by wild-type (A), and O-demethylenation (B), N-dealkylation (C), and N-hydroxylation (D) by Phe[120]Ala mutant CYP2D6 of the different MDAAs.

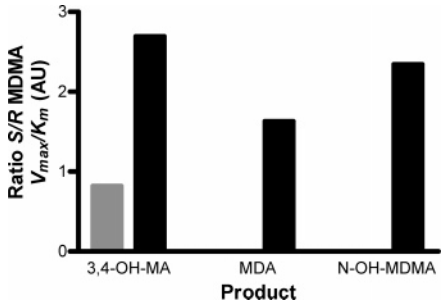

Figure 3. Ratios of *S*-MDMA catalytic efficiency (V_{max}/K_m) over *R*-MDMA catalytic efficiency (V_{max}/K_m) by wild-type (gray) and by Phe[120]Ala mutant CYP2D6 (black) for the products 3,4,-dihydroxy-*N*-alkylamphetamine (3,4-OH-MA), 3,4-methylenedioxyamphetamine (MDA), and 3,4-methylenedioxy-*N*-hydroxy-*N*-alkylamphetamine (*N*-OH-MDMA).

on the fluorescence yield of the compounds and, therefore, it is reasonable that this holds true for the O-demethylenated and N-hydroxylated products of the MDAAs as well.

The turnover rates of MDMA, MDEA, and MDPA were equal for wild-type CYP2D6 (Table 2). The catalytic efficiency (V_{max}/K_m) indicated that MDPA is oxidized most efficiently and MDMA is oxidized least efficiently (Figure 2A). The mutant showed a higher catalytic efficiency in O-demethylenating MDPA over MDMA and MDEA, while the efficiency in N-hydroxylation was the highest for MDMA (Figure 2B−D). MDEA and MDPA were N-dealkylated more efficiently than MDMA. So, elongation of the *N*-alkyl chain leads to an altered catalytic regioselectivity by the mutant enzyme.

Stereoselectivity in MDMA oxidation by wild-type CYP2D6 was hardly found (Figure 3). However, the mutant enzyme showed at least 2-fold lower K_m values for all three products of *S*-MDMA when compared to *R*-MDMA, while the V_{max} values for the products of both enantiomers did not differ (Table 2). Eventually, these changes lead to a different product ratio for the enantiomers: O-demethylenation is more prominent for *S*-MDMA than for *R*-MDMA, followed by N-hydroxylation and N-dealkylation (Figure 3).

NMR Spin Lattice Relaxation Rate Measurements. Enzyme bound MDMA hydrogen atom to heme iron distances were determined by spin lattice relaxation NMR to validate the computationally predicted distances. The ^1H NMR spectrum of MDMA in the presence of glycerol and each of the two enzymes was well resolved; all signals of the different hydrogen atoms were clearly visible (Figure 4). Because the doublet of the C_3-methyl (δ 1.18 ppm) and the singlets of the *N*-methyl (δ 2.61 ppm) and methylene (δ 5.89 ppm) hydrogen atoms could be best quantified and are the most distal groups in MDMA, these were used to determine the substrate orientation in the active site of the two enzymes (inversion recovery spectra shown in the Supporting Information). An increase in T_1 of the MDMA hydrogen atoms was found after reducing the enzymes with dithionite, indicating that the paramagnetic effect of the enzymes was diminished. From T_1, the distances from the methylene, C_3-methyl, and *N*-methyl hydrogen atoms to the heme iron atom were calculated (using eq 2) and tabulated (in Table 3). The fast exchange condition (see the Materials and Methods

Table 3. Hydrogen Atom to Heme Iron Distances (Å) of the MDMA Enantiomers to Wild-Type and Phe[120]Ala Mutant CYP2D6 as Determined by NMR Spin Lattice Relaxation Rate Measurements and by MD Simulations of Neutral and Charged MDMA[a]

		wild-type		Phe[120]Ala	
position	method	*R*-MDMA	*S*-MDMA	*R*-MDMA	*S*-MDMA
methylene (δ 5.89 ppm)	NMR	6.4	6.3	6.4	6.5
	MD (charged)	3.5	3.6	4.6	3.1
	MD (neutral)	4.3	4.5	5.0	5.5
N-methyl (δ 2.61 ppm)	NMR	7.3	7.2	7.5	7.2
	MD (charged)	11.0	10.1	10.1	9.4
	MD (neutral)	5.9	6.5	8.4	6.0
C_3 (δ 1.18 ppm)	NMR	6.9	6.7	6.6	6.7
	MD (charged)	11.8	11.0	8.7	11.5
	MD (neutral)	5.3	6.6	6.9	6.5

[a] NMR derived values are the means of at least two independent measurements with SD less than 5%, as described in the Materials and Methods section. MD simulations derived values are averaged over time and for three individual runs starting from different docking poses, according to eq 4.

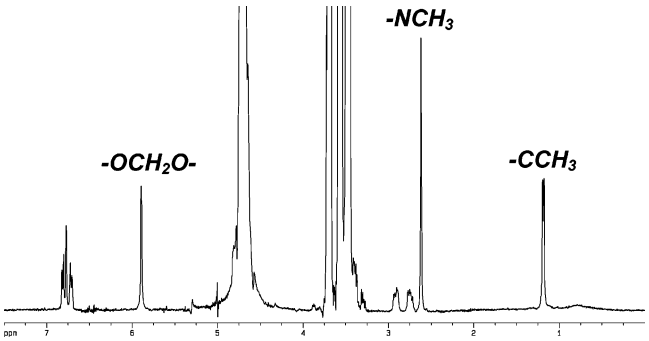

Figure 4. ^{1}H NMR spectrum of 20 mM *R*-MDMA in deuterated KPi−glycerol in the presence of 5 μM Phe[120]Ala mutant CYP2D6 showing the resonance assignments.

section) was validated by measuring the temperature dependence of R_{1P} from 281 K to 307 K (see the Supporting Information). For the three groups of hydrogen atoms studied, there was a linear increase of R_{1P} with an increase in the reciprocal temperature ($1/T$), showing that the exchange between substrate molecules in the enzyme active site and in solution is fast on the NMR time scale. Only minor differences were observed for the hydrogen atoms to iron distances between the enantiomers of MDMA and each of the two enzymes. The measured hydrogen atoms to iron distances indicate that the methylene moiety is closest to the heme iron at about 6.4 Å, the *N*-methyl is the most distal to the heme at about 7.3 Å, and the C_3 hydrogen atoms are at a distance of about 6.7 Å.

Automated Docking Studies. All automatically docked poses of the MDAAs, in two protonation states and in both enzymes, were found to be predominantly within a reactive distance of 6 Å from the heme iron atom (69% and higher, Table 4A). Of these reactive poses, the large majority corresponded to O-demethylenation (62−100%). The relative occurrence of docking poses corresponding to N-dealkylation (0−38%) and N-hydroxylation (0−13%) of the MDAAs was found to be enzyme, stereoisomer, and protonation state dependent. In both enzymes, the neutral forms of the compounds showed the widest range of reactive substrate orientations, whereas the wild-type allowed for more diversity. This observation is in contrast with the experimental finding that wild-type CYP2D6 only catalyzes O-demethylenation, while the Phe[120]Ala mutant allows for alternative product formation.

Three distinct, energetically most favorable automatically docked poses were selected of all MDAAs as starting conformations for MD calculations, and an example of charged *R*-MDMA is shown (Figure 5). These three distinct docked poses could be generally described as one binding orientation corresponding to O-demethylenation, with the substrate nitrogen atom in close contact with Glu[216] (pose 1, generated with AutoDock), another corresponding to O-demethylenation, with the substrate nitrogen atom placed between Glu[216] and Asp[301] (pose 2, generated with GOLD), and one corresponding to N-dealkylation or N-hydroxylation (pose 3, generated with AutoDock). In cases where pose 3 was not observed for the substrate in the charged form (see Table 4A), the corresponding pose of the neutral state was protonated and taken as a starting conformation for MD simulations.

MD Simulations. Simulations of the enzymes with substrates bound in the active site, starting from the three different automatically docked poses, remained stable during 10 ns of unrestrained MD at 300 K, with final atom-positional root-mean-square deviation values of 1.3−3.8 Å. Throughout the simulations, structure determining hydrogen bonds were observed and the majority of the orientations of the substrates in the enzymes were within a reactive distance to the iron atom (74% and higher, Table 4B). The substrates appeared to have considerable freedom within the binding site. Complete reorientation from the initial coordinates was frequently observed, indicating that the unrestrained MD simulations sampled the substrate conformational space sufficiently. The distances between substrate hydrogen atoms and the heme iron atom of wild-type and Phe[120]Ala mutant CYP2D6 were derived for two different protonation states of the MDMA enantiomers by averaging the distances over the three simulations (using eq 4), and these were subsequently compared to experimentally determined distances (Table 3). Relatively large differences in averaged hydrogen atom to iron distances were found within individual MD simulations starting from different substrate docking poses. However, averaged distances of individual MD simulations of the same protonation state and starting from the same docking pose were approximately equal. An exception was the difference in averaged distance of the methylenedioxy hydrogen atoms of both neutral MDMA enantiomers in simulations starting from pose 3 (corresponding to N-demethylation/hydroxylation) in wild-type CYP2D6 (∼7.5 Å) compared to the Phe[120]Ala mutant (∼11.0 Å). Also, the averaged distances derived from all three simulations

Table 4. Distributions of Substrate Orientations Corresponding to Specific Sites of Oxidation (%), According to Automated Docking Studies (A) and MD Simulations (B)[a]

			wild-type					Phe[120]Ala				
substrate			reactive	ODM	NDM	NOH	ωOH	reactive	ODM	NDM	NOH	ωOH
						(**A**) Automated Docking Studies						
MDMA	*R*	charged	100	100	0	0	-	100	100	0	0	-
		neutral	88	86	10	4	-	93	90	3	7	-
	S	charged	92	100	0	0	-	100	100	0	0	-
		neutral	99	73	14	13	-	80	99	0	1	-
MDEA	*R*	charged	91	99	1	0	0	100	99	1	0	0
		neutral	100	91	9	0	0	100	98	2	0	0
	S	charged	69	99	1	0	0	100	99	1	0	0
		neutral	99	78	22	0	0	100	93	7	0	0
MDPA	*R*	charged	70	79	21	0	0	99	99	1	0	0
		neutral	92	62	38	0	0	100	97	3	0	0
	S	charged	74	100	0	0	0	95	62	38	0	0
		neutral	82	99	1	0	0	100	73	27	0	0
						(**B**) MD Simulations						
MDMA	*R*	charged	97	100	0	0	-	89	100	0	0	-
		neutral	77	83	3	12	-	96	69	3	28	-
	S	charged	99	100	0	0	-	100	100	0	0	-
		neutral	80	88	1	11	-	92	64	23	13	-
MDEA	*R*	charged	74	99	0	0	1	64	99	0	0	1
		neutral	95	85	2	2	11	93	71	18	9	2
	S	charged	100	100	0	0	0	76	100	0	0	0
		neutral	82	92	2	6	0	79	61	32	5	2
MDPA	*R*	charged	97	100	0	0	0	99	100	0	0	0
		neutral	97	100	0	0	0	100	58	22	1	20
	S	charged	100	100	0	0	0	98	100	0	0	0
		neutral	100	100	0	0	0	98	99	1	0	0

[a] The columns labeled "reactive" indicate the percentage of all binding orientations that displayed a site of oxidation within 6 Å of the heme iron. The subsequent columns show the distribution of the reactive conformations for the different sites of oxidation, corresponding to O-demethylenation (ODM), N-demethylation (NDM), N-hydroxylation (NOH), and "omega-hydroxylation" (ωOH). The automated docking studies are based on 50 independent AutoDock and GOLD docking runs; the MD simulations are Boltzmann weighted averages over three independent simulations starting from three different docking poses. Substrates were simulated in neutral and charged form.

of individual protonation states were approximately the same for the different MDMA enantiomers in wild-type and Phe[120]Ala mutant CYP2D6. The averaged hydrogen atom to heme iron distances of the neutral MDMA enantiomers agreed well with the distances determined by NMR spin lattice relaxation rate measurements. Apparently, considering the substrates to be neutral describes the experimental situation best. With the exception of the *N*-methyl and C_3 hydrogen atoms of *R*-MDMA in the Phe[120]Ala mutant, all hydrogen atom to heme iron distances calculated from MD simulations of neutral MDMA enantiomers were shorter than the experimentally derived distances. The methylenedioxy hydrogen atom to heme iron distances were slightly lower than those of the *N*-methyl and C_3 hydrogen atoms. In contrast, the averaged *N*-methyl and C_3 hydrogen atom to heme iron distances of the charged MDMA enantiomers violated the experimental distances consistently.

For all MDAAs, differences between the averaged enzyme−substrate interaction energies calculated using SCORE were within 3 kJ mol^{-1} ($\sim kT$) for all three MD simulations of the same protonation states and within 5 kJ mol^{-1} for all six MD simulations. The relative weights of the MD simulations of the three starting orientations used in the Boltzmann averaging (eq 5, see the Materials and Methods section) over the simulations ranged between 0.11 and 0.54.

Already during the equilibration time or soon after the start of the MD simulations with charged MDAAs, reorientation of pose 3 into pose 1 (corresponding to O-demethylenation) occurred. In the case of MDEA, this led to nonreactive binding orientations outside of the binding pocket, forming a hydrogen bond between its protonated nitrogen and the carboxylate group of Glu[216] (Table 4B and Figure 5). Relatively high probabilities of O-demethylenation poses were found for neutral MDAAs (>58%), although orientations corresponding to N-demethylation/hydroxylation were also observed (except for MDPA in wild-type CYP2D6). N-demethylation or N-hydroxylation of neutral MDAAs had significantly higher probabilities in the Phe[120]Ala mutant than in wild-type CYP2D6. Furthermore, substrate dependent catalytic regioselectivity was observed for the mutant: elongation of the *N*-alkyl chain led to a decreased N-hydroxylation efficiency with an optimal N-dealkylation efficiency for MDEA (Table 4B). These trends were equal to those found experimentally and became even more pronounced when the MDAAs were averaged over enantiomers and protonation states and Boltzmann weighted (Figure 6).

Significant stereoselective differences in the probabilities of O-demethylenation vs N-demethylation/hydroxylation were not observed for wild-type CYP2D6. The Phe[120]Ala mutant, however, did in all cases discriminate the enantiomers of the neutral MDAAs. Differences between the probabilities of N-demethylation and N-hydroxylation of MDMA enantiomers were found, and *R*-MDPA was found in orientations leading to N-demethylation and ω-hydroxylation more often than *S*-MDPA (Table 4B).

Enzyme−substrate interactions observed in the MD simulations of neutral MDAAs showed a significant decrease in van der Waals/aromatic interactions with residue 120 in the Phe[120]Ala mutant compared to wild-type CYP2D6 (Table 5). Furthermore, a small decrease

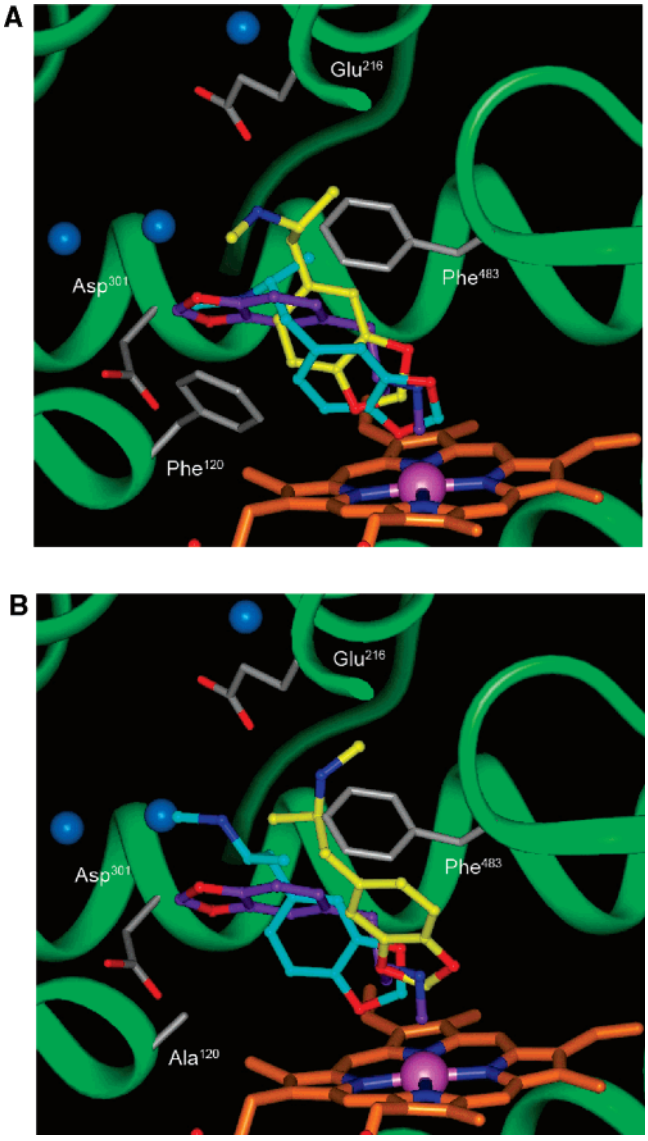

Figure 5. MD simulations starting orientations of charged *R*-MDMA, generated by automated docking studies in wild-type (A) and Phe[120]Ala mutant (B) CYP2D6 homology models. Two orientations are corresponding to O-demethylenation, with the substrate nitrogen atom either in close contact with Glu[216] (pose 1, in yellow) or placed between Glu[216] and Asp[301] (pose 2, in cyan). A third orientation is corresponding to N-demethylation or N-hydroxylation (pose 3, in purple). Water oxygen atoms, as predicted by GRID (see Materials and Methods section), are depicted in blue.

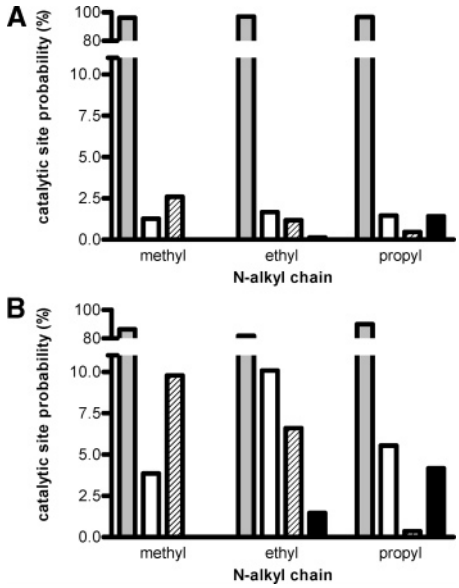

Figure 6. Probabilities (%) of reactive binding orientations corresponding to O-demethylenation (gray), N-dealkylation (white), N-hydroxylation (diagonal stripes), and ω-hydroxylation (black) of the MDAAs in wild-type (A) and in Phe[120]Ala mutant (B) CYP2D6, as derived from 12 MD simulations. Shown are the Boltzmann weighted averages of two different protonation states and three different docking poses (examples in Figure 5), assuming a 1:1 ratio between *R*- and *S*-enantiomers.

Table 5. Enzyme−Substrate Interactions (%) during MD Simulations[a]

		wild-type		Phe[120]Ala	
substrate		VdW/arom Phe[120]	H-bond Glu[216]	VdW/arom Ala[120]	H-bond Glu[216]
MDMA	*R*	81	65	12	54
	S	80	69	23	47
MDEA	*R*	55	51	2	46
	S	66	70	1	57
MDPA	*R*	71	74	5	52
	S	81	52	7	61

[a] Enzyme−substrate interactions during the MD simulations were monitored in terms of the occurrence of atom−atom distances of 3.5 Å or less between the Phe/Ala[120] side chain and the MDAA ring system, representing aromatic/van der Waals interactions, and hydrogen bonds between the Glu[216] carboxylate oxygen atoms and the MDAA nitrogen atom. Values of neutral and charged substrates were averaged.

in hydrogen-bond interactions with the carboxylic acid of Glu[216] was observed for the Phe[120]Ala mutant as a direct result of the relatively high probability of binding orientations corresponding to N-dealkylation or N-hydroxylation. In both wild-type and Phe[120]Ala mutant CYP2D6, however, hydrogen-bond interactions were found to be significantly decreased for neutral MDAAs (up to 23% on average for each enantiomer) when compared to charged MDAAs (up to 92% on average for each enantiomer). During the MD simulations, water molecules were primarily observed to fill the part of the active site which is connected with a so-called "water channel", [31] which was already partially occupied by predicted water molecules in the automated docking starting structures (Figure 5). These water molecules were found to form H-bonds with the substrate. At most, one water molecule was observed in other regions of the active site.

Discussion

The primary aim of this study was to develop an integrated molecular modeling approach to analyze substrate oxidation by CYP2D6. When regioselectivity and stereoselectivity in metabolic oxidation and the effect of enzyme active site mutations can be visualized and quantified using a series of related compounds, such an approach could be a useful tool in the rationalization and prediction of metabolism. Using this approach, the experimentally determined binding modes and the product formation of a series of MDAAs by wild-type and Phe[120]Ala mutant CYP2D6 could be rationalized.

Substrate Binding Orientations. In the present study, molecular modeling was used to explain the

apparent discrepancy between experimentally observed differences in regioselective oxidation and the stereoselective preference by the Phe[120]Ala mutant toward MDMA (Figure 1) and the average substrate orientation in the mutant and wild-type active sites as determined by NMR spin lattice relaxation rate measurements (Table 3). The average hydrogen atom to iron distances calculated from the T_1 of the MDMA enantiomers in both enzymes were equal, with the methylene moiety in both cases closest to the heme iron atom. Although the distances between the hydrogen atoms at potential sites of oxidation in MDMA and the heme iron atom were somewhat larger than comparable distances found in CYP X-ray structures (4−6 Å), they were within the range of distances determined in other NMR studies.[27−30] This difference can be explained by the fact that experimentally determined distances are averages of all possible substrate orientations during access to, residence in, and exit from the active site. As a result, they contain more information than just that of a reactive substrate orientation. NMR spin lattice relaxation rate measurements have been used before to determine the orientation of codeine in CYP2D6, where the measured hydrogen atoms to iron atom matched the orientation expected from codeine's metabolic profile.[28] Codeine is a more rigid and bulky substrate than MDMA, which may explain the good match. Caffeine, a small and low affinity substrate of CYP1A2, was also a subject of NMR spin lattice relaxation rate measurements, but the orientation of caffeine found did not match the metabolic profile.[30] From other experimental studies, it is known that substrates can be quite mobile in CYP active sites,[32] and the existence of multiple substrate binding modes and substrate mobility in CYP2D6 is clearly supported by our molecular modeling studies. Averaged distances derived from the present studies, considering three distinct automatically docked substrate binding modes of the MDAAs in combination with long MD simulations, were in good agreement with the experimentally determined metabolic profiles when considering the MDAAs to be in their neutral form (Table 3). Still, this does not explain the experimentally observed change in regioselective oxidation and stereoselective preference of the Phe[120]Ala mutant toward MDMA compared to the wild-type. So, it is likely that a small substrate like MDMA is very mobile in the CYP2D6 active site and that the reactivity of possible sites of oxidation also determines which products are being formed.

Regioselectivity and Stereoselectivity in Oxidation. Experimentally observed trends in regioselectivity in the oxidation of the MDAAs by wild-type and Phe[120]-Ala mutant CYP2D6 (Table 2) were in good agreement with the relative probabilities of different binding modes of the MDAAs observed in the MD simulations (Table 4B). In the wild-type enzyme, only O-demethylenation was observed experimentally, while in the Phe[120]Ala mutant N-demethylation and N-hydroxylation also occurred. The molecular modeling studies showed that N-demethylation/hydroxylation probabilities for neutral MDAAs were significantly higher in the Phe[120]Ala mutant than in the wild-type enzyme (Table 4B). Both the experimental and modeling studies showed a decreased N-hydroxylation efficiency with elongation of the *N*-alkyl chain and that the highest MDA formation efficiency was that of MDEA. Stereoselectivity in oxidation of MDMA by wild-type CYP2D6 was hardly found experimentally or predicted by molecular modeling. However, the experimentally observed preference for *S*-MDMA by the Phe[120]Ala mutant could not be rationalized by molecular modeling. This may be due to the fact that the stereoselectivity is predominantly caused by a difference in K_m and not in V_{max}, while affinities of the substrates to the enzymes were not predicted in a rigorous manner in this study. On the other hand, the small violations of the calculated to the experimentally determined hydrogen atom to iron distances for neutral *R*-MDMA bound to the Phe[120]Ala mutant do indicate that this enantiomer experiences more difficulties in finding its optimum orientation in the binding pocket.

Influence of Phe[120]Ala Mutation on Oxidation Reactions. By removing the phenyl ring of Phe[120], more space is created in the active site of CYP2D6 and a specific aromatic interaction point is eliminated.[18] From the MD simulations, it became clear that this space was not occupied by the MDAAs or by water molecules, but that critical substrate interactions were lost after mutating Phe[120] into an alanine (Table 5). This observation and the fact that the stereo- and regioselectivities of the mutant enzyme differed from those of the wild-type show that Phe[120] is important for specific interactions with the MDAAs in CYP2D6. There is not sufficient space in the active sites of wild-type or the Phe[120]Ala mutant CYP2D6 to accommodate two molecules of the MDAAs at the same time. However, it could be possible that two substrate molecules bind simultaneously to different parts of the protein, e.g., in the active site and in substrate access channels[31] or in a peripheral binding site.[10]

Combination of Automated Docking and MD Simulations. In earlier studies, it was shown that automated docking can successfully be applied to predict sites of oxidation by CYPs.[21] In contrast, the current study shows that automated docking alone is not suitable for accurate determination of relative probabilities of different substrate binding modes and for discrimination between substrates and enzymes of high similarity, such as regio/stereoisomers and mutants of enzymes. To reproduce the experimental data, which are an average over many different substrate and enzyme orientations in time, a dynamic treatment of both substrate and enzyme is required. Only when averaging over different positions and orientations was taken into account could experimentally determined substrate hydrogen atoms to heme iron atom distances be reproduced accurately. The experimentally observed differences in substrate oxidation by wild-type and Phe[120]Ala mutant CYP2D6 could only be explained from the different binding modes observed in the MD simulations. Multiple and extensive MD simulations are needed to catch these subtle differences between substrates, enzyme structures, and their dynamics.

Substrate Protonation States. The molecular modeling was performed with neutral and charged substrates because this difference markedly influenced the binding and mobility of the MDAAs in the active site of the two enzymes. Even though the MDAAs in physiological solution will occur predominantly in their charged form, the preferred protonation state within the

binding pocket can differ significantly; thus, reductions of apparent pK_a values for substrates upon binding to CYP2D6 of up to 2 pH units have been reported.[26] From a direct comparison between the experimentally derived hydrogen atom to heme iron distances and the computationally determined values, it became clear that the MD simulations reproduced the experimental data best when the MDAAs were represented in their neutral form.

Conclusions

The approach of combining automated docking and MD simulations in a protein model was a successful way to rationalize the oxidative metabolism of a series of 3,4-methylenedioxy-*N*-alkylamphetamines (MDAAs) by CYP2D6. Differences in oxidative metabolism of these closely related substrates could be predicted in details such as regioselectivity and stereoselectivity. Furthermore, the effects of the active site Phe[120]Ala mutation on the selectivity of the substrate could be rationalized. The presented integrated modeling method is a promising tool in the prediction of the metabolic properties of new (druglike) compounds with respect to interactions with CYP2D6 and might be applicable to other drug metabolizing enzymes as well.

Materials and Methods

Materials. The pSP19T7LT plasmid containing human 2D6 with a C-terminal His_6-tag bicistronically coexpressed with human NADPH-cytochrome P450 reductase was kindly provided by Prof. Dr. Ingelman-Sundberg. 3,4-Methylenedioxy-*N*-alkylamphetamines (MDAAs) were synthesized as described before.[33,34] *S*- and *R*-MDMA·HCl were obtained from the Division of Neuroscience and Behavioral Research of the National Institute on Drug Abuse (Bethesda, MD). Emulgen 911 was purchased at KAO Chemicals (Tokyo, Japan). Ni-NTA-agarose was from Qiagen (Westburg, Leusden, The Netherlands). All other chemicals were of analytical grade and obtained from standard suppliers.

Expression and Purification of CYP2D6. Both the Phe[120]Ala mutant and the wild-type pSP19T7LT plasmids were transformed into *Escherichia coli*, strain JM109. Expression and membrane isolation were carried out as described.[18] Membranes were resuspended in 0.4% of the original culture volume of a KPi−glycerol buffer (50 mM potassium phosphate buffer, pH 7.4, 10% glycerol), and CYP contents were determined by CO-difference spectra.[35]

Enzymes were solubilized from membranes by stirring in KPi−glycerol supplemented with 0.5% Emulgen 911 for 2 h at 4 °C. Insoluble parts were removed by centrifugation (60 min, 120000*g* at 4 °C). The supernatant was incubated, while gently rocking, with Ni-NTA-agarose for 30 min at 4 °C. The Ni-NTA-agarose was retained in a polypropylene tube with a porous disk (Pierce, Perbio Science, Ettenleur, The Netherlands) and washed with a KPi−glycerol buffer containing 2 mM histidine. CYP2D6 was eluted with 0.2 M histidine. After overnight dialysis in the KPi−glycerol buffer, the sample was concentrated on a Vivaspin 20 filtration tube (10.000 MWCO PES, Sartorius, Nieuwegein, The Netherlands). For NMR spin lattice relaxation rate measurements, the buffer was exchanged for a deuterated KPi−glycerol buffer by repeated rounds of adding a larger volume of deuterated buffer and concentrating. The deuterated KPi−glycerol buffer was made by repeated rounds of evaporating water or D_2O from a KPi buffer and dissolving the residue again in D_2O. Then 5% glycerol was added, and traces of iron were removed with Chelex 100 (Biorad, Richmond, CA).

Optical Titrations. Dissociation constants of substrates to the enzymes were determined by spectral titration, according to the method of Jefcoate.[36,37] Spectra were taken at room temperature on a Pharmacia Ultrospec 2000 spectrometer. In short, 1 mL of 0.5 μM purified enzyme in a KPi−glycerol buffer was divided over two cuvettes; to the first, 5 μL of a 1 mM solution of compound in the same buffer was added, and to the second, the same volume of just buffer was added. Difference spectra from 350 to 450 nm were taken before and after each addition of compound. The difference in absorbance at 390 and 425 was plotted against the substrate concentration to estimate the dissociation constant (K_s) using eq 1 in Graph Pad Prism 4.0 software, where B is the absorbance difference (390−425) and B_{max} is the absorbance difference when [S] = ∞.

$$B = \frac{B_{max}[S]}{K_s + [S]} \quad (1)$$

Metabolism of MDAAs. Metabolic reactions were carried out in 200 μL of 50 mM KPi (pH 7.4) and 5 mM $MgCl_2$ supplemented with 10 concentrations ranging from 0 to 200 μM of one of the MDAAs and *E. coli* membranes corresponding to 25 nM wild-type or Phe[120]Ala mutant CYP2D6. After 5 min of preincubation at 37 °C, the reactions were initiated with an NADPH regenerating system, resulting in final concentrations of 0.2 mM NADPH, 0.3 mM glucose-6-phosphate, and 0.4 units mL^{-1} glucose-6-phosphate dehydrogenase. The reaction was allowed to proceed for 10 min before it was stopped by the addition of 20 μL of 23% $HClO_4$. After centrifugation (10 min, 6800*g*), 30 μL aliquots of the supernatant were analyzed by high-performance liquid chromatography (HPLC). To measure O-demethylenation, analytes were separated isocratically using a C18 column (Phenomenex Luna 5u 150 mm × 4.6 mm), with a mobile phase consisting of 22% acetonitrile and 0.1% triethylamine, set to pH 3 with $HClO_4$ at a flow rate of 0.6 mL min^{-1}. Other oxidation products were found using the same column with a gradient (A, 5% ACN with 20 mM ammonium acetate; B, 90% ACN with 10 mM ammonium acetate). All oxidation products were detected by fluorescence (λ_{ex} = 280 nm, λ_{em} = 320 nm) and identified by liquid chromatography−mass spectroscopy (LC-MS). Peak areas of all products were quantified with Shimadzu Class VP 4.3 software and analyzed using nonlinear regression with one site binding in Graph Pad Prism 3.0.

LC-MS. To identify the metabolic products of the MDAAs, incubations were carried out for 15 min as described above with 100 μM MDMA, MDEA, or MDPA and *E. coli* membranes corresponding to 50 nM wild-type or Phe[120]Ala mutant CYP2D6. Volumes of 100 μL of supernatant were injected and separated using a C18 column (Phenomenex Luna 5u 150 mm × 4.6 mm) with a flow rate of 0.6 mL min^{-1} and analyzed by MS. The analytes were eluted using a gradient starting with a 5% ACN eluens, supplemented with 20 mM ammonium acetate for 7 min, then, increasing linearly to 90% ACN with 10 mM ammonium acetate in 14 min, and remaining there for 5 min. APCI positive ionization was used on a LCQ Deca mass spectrometer (Thermo Finnigan, Breda, The Netherlands) with a vaporizer temperature of 450 °C, N_2 as a sheath (40 psi) and an auxiliary gas (10 psi), a needle voltage of 6000 V, and a heated capillary at 150 °C.

Products of MDMA metabolism: 3,4-OH-MA (t_R 9.5 min, *m/z* 182, MS/MS *m/z* 151), MDA (t_R 17.0 min, *m/z* 180, MS/MS *m/z* 163), and *N*-OH-MDMA (t_R 20.4 min, *m/z* 210, MS/MS *m/z* 163). Products of MDEA metabolism: 3,4-OH-EA (t_R 13.0 min, *m/z* 196, MS/MS *m/z* 151), MDA (t_R 17.0 min, *m/z* 180, MS/MS *m/z* 163), *N*-OH-MDEA (t_R 21.6 min, *m/z* 224, MS/MS *m/z* 163), and a fourth product for the mutant (t_R 18.5 min, *m/z* 222, MS/MS *m/z* 163). Products of MDPA metabolism: 3,4-OH-PA (t_R 16.0 min, *m/z* 210, MS/MS *m/z* 151), MDA (t_R 17.0 min, *m/z* 180, MS/MS *m/z* 163), *N*-OH-MDPA (t_R 23.4 min, *m/z* 238, MS/MS *m/z* 163), and a fourth product for the mutant (t_R 19.2 min, *m/z* 254, no fragmentation observed).

NMR Spin Lattice Relaxation Rate Measurements. Distances from substrate hydrogen atoms to the enzyme heme iron atom were calculated from their longitudinal relaxation rates determined using ^1H NMR.[27−30] ^1H NMR measurements

were performed on a Bruker Avance 400 MHz spectrometer; signals were referenced to HDO at 4.75 ppm. Longitudinal relaxation times (T_1) of substrate hydrogen atoms were measured with a standard inversion recovery sequence of 180°−τ−90°. The spectra were recorded with 20 values of τ, ranging from 0.1 to 12.5 s, and a relaxation delay of 5−10 times T_1. The temperature was kept at 300 K, except for in the variable temperature experiments. T_1 was determined by plotting peak areas against delay times, τ, and by exponential fitting ($I_t = A + Be^{-\tau/T_1}$) with Bruker XWINNMR software. The measured T_1 was transformed into the longitudinal paramagnetic relaxation rate (R_{1P}) according to eq 2. $T_{1,Fe^{3+}}$ is the relaxation time

$$R_{1P} = (T_{1,Fe^{3+}})^{-1} - (T_{1,Fe^{2+}+CO})^{-1} \quad (2)$$

of substrate hydrogen atoms in the presence of ferric enzymes, and $T_{1,Fe^{2+}+CO}$ is the relaxation time in the presence of ferrous CO-bound enzymes. The hydrogen atoms to iron atom distance, r^{NMR}, can be calculated from R_{1P} using the simplified Solomon and Bloembergen equation[27,38] (eq 3)

$$r^{NMR} = C(\alpha R_{1P} F(\tau_c))^{1/6} \quad (3)$$

where C is a constant taking into account the spin state as well as other nuclear and electronic factors, with a value of 813 for high spin CYP, [30] and α is the fraction of enzyme-bound substrate, determined as the ratio of the concentration of enzyme and the sum of the substrate concentration and its spectral dissociation constant (K_s). $F(\tau_c)$ is a function of the correlation time, τ_c, for which the value of 3×10^{-10} s is taken, as determined for CYP2D6 by others.[28] In the calculations of hydrogen atoms to heme distances according to eqs 2 and 3, the assumption has been made that on the NMR time scale there is a fast exchange between substrate molecules in solution and in the enzyme active site. This was verified by measuring the temperature dependence of $1/T_1$, which should show a linear increase with the reciprocal value of the temperature.[29,30]

In a typical experiment, 5 μM enzyme and 20 mM substrate were used in a volume of 500 μL. Recording the spectra for the determination of relaxation times with oxidized enzyme took about an hour; then, sodium dithionite was added, and the sample was treated for 30 s with CO to do the measurements with the reduced CO-bound enzyme.

Homology Modeling. A protein homology model of CYP2D6 was constructed based on the crystal structures of dimethylsulfophenazole derivative and diclofenac-bound rabbit CYP2C5 (PDB codes 1N6B and 1NR6, respectively).[39,40] Homology modeling, model refinement, and model validation were performed according to the approach described previously.[12] In short, one hundred CYP2D6 models were generated with the restraint-based comparative modeling program Modeler,[41] using the same amino acid alignment as before.[12] Subsequently, three models were selected with the best loop conformations, as determined by visual inspection, stereochemical parameters using PROCHECK,[42] and side-chain environment using Errat[43] and Verify3D.[44] Homology models had approximately the same protein quality check scores as the crystal structure templates. Finally, one single model was selected which could accommodate codeine best in the experimental binding orientation.[28] This final model was validated on its ability to reproduce substrate binding orientations corresponding to metabolic profiles with AutoDock,[45] FlexX,[46] and GOLD[47] automated docking studies (De Graaf, unpublished results). The final model of wild-type CYP2D6 was used as a template for modeling of the Phe[120]Ala mutant. The Phe residue at position 120 was mutated to Ala using the homology module of Insight II (Biosym, San Diego, CA), after which an energy minimization and a 1 ps MD simulation with position restraints on the protein backbone were carried out as described in MD Simulations of the Results section.

Automated Docking Studies. The *R*- and *S*-enantiomers of MDMA, MDEA, and MDPA in their neutral (basic) and charged (acidic) forms were docked into the active site of the CYP2D6 homology model using AutoDock and GOLD. Active site water molecules, predicted using a protocol based on the program GRID[48] and a ligand-based cut off, were included. The preparation of enzyme and substrate structures in the automated docking studies was performed using default settings and predicted water molecules, as described before.[21] For each substrate, 50 independent AutoDock and GOLD docking runs were performed using default parameter values. Docking poses generated by both docking algorithms were clustered (maximum root-mean-square differences between members of the cluster of 1 Å) and rescored with the SCORE scoring function.[49] The three energetically most favorable, distinct docking poses of each MDAA species were selected as starting structures for MD calculations, yielding in total 12 (3 docking poses times 2 enatiomers times 2 protonation states) simulations for each substrate in both wild-type and Phe[120]Ala mutant CYP2D6.

MD Simulations. Substrate conformations selected from the automated docking studies were used as starting structures for MD simulations, using the GROMACS molecular simulation package[50] and the GROMOS-96 force field, parameter set 43A1.[51,52] Heme parameters were taken from this parameter set, and additionally, a covalent bond was defined between the heme iron atom and the sulfur atom of Cys[443] with an ideal bond distance of 0.240 nm. The enzyme, including substrate and heme, was energy minimized in a vacuum using the steepest descent method, first, with harmonic position restraints using a force constant of 1000 kJ mol^{-1} nm^{-2} on all non-hydrogen atoms and, then, without position restraints. Subsequently, preequilibrated water was added in a dodecahedral box with a minimum distance of 1 nm between the enzyme and box edges, followed by minimization. For 1 ps, the water was allowed to relax, while the whole enzyme was position restrained. Then, first, only the side chains of the residues not involved in substrate binding were released for 1 ps, and next, also the backbone of these residues was released for 10 ps. Finally, only the backbone of the binding residues was restrained for 100 ps. The equilibration scheme was followed by an unrestrained 10 ns MD production run. MD simulations were carried out with a time step of 2 fs, a twin-range cutoff of 0.8/1.4 nm, and a relative dielectric constant of 1.0. The LINCS algorithm was used to constrain the length of all covalent bonds.[53] Pressure was maintained at 1 bar and temperature at 300 K by weak coupling to an external bath,[54] with relaxation times of 0.1 and 1.0 ps, respectively. Coordinates were saved at a 1.0 ps interval for subsequent analysis. Enzyme−substrate interactions were estimated using the SCORE scoring function and averaged over the trajectories.

Analysis of MD Simulations. Hydrogen atoms to iron atom distances, r^{MD}, for different protonation states of the MDMA enantiomers were derived from MD simulations by averaging distances (r) observed in the three independent simulations with different starting positions as

$$r^{MD} = (\langle r^{-6} \rangle)^{-1/6} \quad (4)$$

These distances could be directly compared to the experimentally obtained distances, r^{NMR} (eq 3).

Sites of oxidation were predicted based on enzyme−substrate conformations generated by automated docking and MD simulations. Distances of 6.0 Å or less between the heme iron and an atom in the substrate (e.g., corresponding to O-demethylenation, N-dealkylation, N-hydroxylation, or ω-hydroxylation) were considered as reactive in the sense that activation of the C−H bond by the heme-Fe−O moiety is possible.[55] Site of oxidation predictions were performed to determine both substrate reactivity (expressed in the number of reactive MD configurations out of the total) and regioselectivity. The catalytic regioselectivity was calculated by determining which site of oxidation was closest to the heme iron atom for each reactive docking pose or MD configuration. Enzyme−substrate interactions during the MD simulations were monitored in terms of the occurrence of atom−atom distances of 3.5 Å or less between the Phe/Ala[120] side chain and the MDAA ring system (representing aromatic/van der

Waals interactions) and hydrogen bonds between the Glu[216] carboxylate oxygen atoms and the MDAA N-atom. Substrate reactivity, regioselectivity, and enzyme−substrate interactions were calculated for any given protonation state and stereo- and regioisomer, as a Boltzmann weighted average over the three independent MD simulations with different substrate starting orientations. The average of an individual simulation i was weighted by a relative probability, p_i, which was calculated from the average enzyme−substrate interaction estimates as obtained from the program SCORE (E^i_{SCORE}).

$$p_i = (e^{-\Delta E^i_{\mathrm{SCORE}}/k_B T})/(\sum_i e^{-\Delta E^i_{\mathrm{SCORE}}/k_B T}) \quad (5)$$

In this equation, k_B is the Boltzmann constant (8.3441 kJ mol^{-1} K^{-1}), and T is the temperature (300 K).

Acknowledgment. We thank Prof. Dr. Magnus Ingelman-Sundberg and Dr. Mats Hidestrand for providing the pSP19T7LT plasmid containing CYP2D6 and the human NADPH-CYP reductase. We thank Dr. Hari Sing from the NIDA-NIH for providing the MDMA enantiomers. We thank Ed Groot and Jon de Vlieger for technical assistance.

Supporting Information Available: Figures showing the ^{1}H NMR spectra of racemic MDMA with varying values of τ and the temperature dependence of T_1 for specified hydrogen atoms of MDMA in wild-type CYP2D6. This material is available free of charge via the Internet at http://pubs.acs.org.

References

(1) Goeptar, A. R.; Scheerens, H.; Vermeulen, N. P. E. Oxygen and xenobiotic reductase activities of cytochrome P450. *Crit. Rev. Toxicol.* **1995**, *25*, 25−65.
(2) Guengerich, F. P. Cytochrome P450: what have we learned and what are the future issues? *Drug Metab. Rev.* **2004**, *36*, 159−197.
(3) Shimada, T.; Yamazaki, H.; Mimura, M.; Inui, Y.; Guengerich, F. P. Interindividual variations in human liver cytochrome P450 enzymes involved in the oxidation of drugs, carcinogens and toxic chemicals: studies with liver microsomes of 30 Japanese and 30 Caucasians. *J. Pharmacol. Exp. Ther.* **1994**, *270*, 414−423.
(4) Bertilsson, L.; Dahl, M. L.; Dalen, P.; Al-Shurbaji, A. Molecular genetics of CYP2D6: clinical relevance with focus on psychotropic drugs. *Br. J. Clin. Pharmacol.* **2002**, *53*, 111−122.
(5) Zanger, U. M.; Raimundo, S.; Eichelbaum, M. Cytochrome P450 2D6: overview and update on pharmacology, genetics, biochemistry. *Naunyn-Schmiedeberg's Arch. Pharmacol.* **2004**, *369*, 23−37.
(6) Oscarson, M. Pharmacogenetics of drug metabolising enzymes: importance for personalised medicine. *Clin. Chem. Lab. Med.* **2003**, *41*, 573−580.
(7) Ingelman-Sundberg, M. Pharmacogenetics of cytochrome P450 and its applications in drug therapy: the past, present and future. *Trends Pharmacol. Sci.* **2004**, *25*, 193−200.
(8) Williams, P. A.; Cosme, J.; Sridhar, V.; Johnson, E. F.; McRee, D. E. Mammalian microsomal cytochrome P450 monooxygenase: structural adaptations for membrane binding and functional diversity. *Mol. Cells* **2000**, *5*, 121−131.
(9) Williams, P. A.; Cosme, J.; Ward, A.; Angove, H. C.; Vinkovic, D. M.; Jhoti, H. Crystal structure of human cytochrome P450 2C9 with bound warfarin. *Nature* **2003**, *424*, 464−468.
(10) Williams, P. A.; Cosme, J.; Vinkovic, D. M.; Ward, A.; Angove, H. C.; Day, P. J.; Vonrhein, C.; Tickle, I. J.; Jhoti, H. Crystal structures of human cytochrome P450 3A4 bound to metyrapone and progesterone. *Science* **2004**, *305*, 683−686.
(11) de Graaf, C.; Vermeulen, N. P. E.; Feenstra, K. A. Cytochrome P450 in silico: an integrative modeling approach. *J. Med. Chem.* **2005**, *48*, 2725−2755.
(12) Venhorst, J.; ter Laak, A. M.; Commandeur, J. N.; Funae, Y.; Hiroi, T.; Vermeulen, N. P. Homology modeling of rat and human cytochrome P450 2D (CYP2D) isoforms and computational rationalization of experimental ligand-binding specificities. *J. Med. Chem.* **2003**, *46*, 74−86.
(13) Kemp, C. A.; Flanagan, J. U.; van Eldik, A. J.; Marechal, J. D.; Wolf, C. R.; Roberts, G. C.; Paine, M. J.; Sutcliffe, M. J. Validation of model of cytochrome P450 2D6: an in silico tool for predicting metabolism and inhibition. *J. Med. Chem.* **2004**, *47*, 5340−5346.
(14) Ellis, S. W.; Hayhurst, G. P.; Smith, G.; Lightfoot, T.; Wong, M. M.; Simula, A. P.; Ackland, M. J.; Sternberg, M. J.; Lennard, M. S.; Tucker, G. T.; et al. Evidence that aspartic acid 301 is a critical substrate-contact residue in the active site of cytochrome P450 2D6. *J. Biol. Chem.* **1995**, *270*, 29055−29058.
(15) Guengerich, F. P.; Hanna, I. H.; Martin, M. V.; Gillam, E. M. J. Role of glutamic acid 216 in cytochrome P450 2D6 substrate binding and catalysis. *Biochemistry* **2003**, *42*, 1245−1253.
(16) Paine, M. J.; McLaughlin, L. A.; Flanagan, J. U.; Kemp, C. A.; Sutcliffe, M. J.; Roberts, G. C.; Wolf, C. R. Residues glutamate 216 and aspartate 301 are key determinants of substrate specificity and product regioselectivity in cytochrome P450 2D6. *J. Biol. Chem.* **2003**, *278*, 4021−4027.
(17) Flanagan, J. U.; Marechal, J. D.; Ward, R.; Kemp, C. A.; McLaughlin, L. A.; Sutcliffe, M. J.; Roberts, G. C.; Paine, M. J.; Wolf, C. R. Phe120 contributes to the regiospecificity of cytochrome P450 2D6: mutation leads to the formation of a novel dextromethorphan metabolite. *Biochem. J.* **2004**, *380*, 353−360.
(18) Keizers, P. H. J.; Lussenburg, B. M. A.; de Graaf, C.; Mentink, L. M.; Vermeulen, N. P. E.; Commandeur, J. N. M. Influence of phenylalanine 120 on cytochrome P450 2D6 catalytic selectivity and regiospecificity: crucial role in 7-methoxy-4-(aminomethyl)-coumarin metabolism. *Biochem. Pharmacol.* **2004**, *68*, 2263−2271.
(19) Ekins, S.; de Groot, M. J.; Jones, J. P. Pharmacophore and three-dimensional quantitative structure activity relationship methods for modeling cytochrome P450 active sites. *Drug Metab. Dispos.* **2001**, *29*, 936−944.
(20) Vermeulen, N. P. E. Prediction of drug metabolism: the case of cytochrome P450 2D6. *Curr. Top. Med. Chem.* **2003**, *3*, 1227−1239.
(21) de Graaf, C.; Pospisil, P.; Pos, W.; Folkers, G.; Vermeulen, N. P. E. Binding mode prediction of cytochrome P450 and thymidine kinase protein−ligand complexes by consideration of water and rescoring in automated docking. *J. Med. Chem.* **2005**, *48* (7), 2308−2318.
(22) Harris, D.; Loew, G. Prediction of regiospecific hydroxylation of camphor analogs by cytochrome-P450(Cam). *J. Am. Chem. Soc.* **1995**, *117*, 2738−2746.
(23) Harris, D. L.; Loew, G. H. Investigation of the proton-assisted pathway to formation of the catalytically active, ferryl species of P450s by molecular dynamics studies of P450eryF. *J. Am. Chem. Soc.* **1996**, *118*, 6377−6387.
(24) Keseru, G. M.; Kolossvary, I.; Bertok, B. Cytochrome P-450 catalyzed insecticide metabolism. Prediction of regio- and stereoselectivity in the primer metabolism of carbofuran: A theoretical study. *J. Am. Chem. Soc.* **1997**, *119*, 5126−5131.
(25) Park, J. Y.; Harris, D. Construction and assessment of models of CYP2E1: Predictions of metabolism from docking, molecular dynamics, and density functional theoretical calculations. *J. Med. Chem.* **2003**, *46*, 1645−1660.
(26) Miller, G. P.; Hanna, I. H.; Nishimura, Y.; Guengerich, F. P. Oxidation of phenethylamine derivatives by cytochrome P450 2D6: the issue of substrate protonation in binding and catalysis. *Biochemistry* **2001**, *40*, 14215−14223.
(27) van de Straat, R.; de Vries, J.; de Boer, H. J.; Vromans, R. M.; Vermeulen, N. P. E. Relationship between paracetamol binding to and its oxidation by two cytochromes P-450 isozymes—a proton nuclear magnetic resonance and spectrophotometric study. *Xenobiotica* **1987**, *17*, 1−9.
(28) Modi, S.; Paine, M. J.; Sutcliffe, M. J.; Lian, L. Y.; Primrose, W. U.; Wolf, C. R.; Roberts, G. C. A model for human cytochrome P450 2D6 based on homology modeling and NMR studies of substrate binding. *Biochemistry* **1996**, *35*, 4540−4550.
(29) Poli-Scaife, S.; Attias, R.; Dansette, P. M.; Mansuy, D. The substrate binding site of human liver cytochrome P450 2C9: an NMR study. *Biochemistry* **1997**, *36*, 12672−12682.
(30) Regal, K. A.; Nelson, S. D. Orientation of caffeine within the active site of human cytochrome P450 1A2 based on NMR longitudinal (T1) relaxation measurements. *Arch. Biochem. Biophys.* **2000**, *384*, 47−58.
(31) Wade, R. C.; Winn, P. J.; Schlichting, I.; Sudarko A survey of active site access channels in cytochromes P450. *J. Inorg. Biochem.* **2004**, *98*, 1175−1182.
(32) Prasad, S.; Mitra, S. Role of protein and substrate dynamics in catalysis by *Pseudomonas putida* cytochrome P450cam. *Biochemistry* **2002**, *41*, 14499−14508.
(33) Braun, U.; Shulgin, A. T.; Braun, G. Centrally active N-substituted analogues of 3,4-methylenedioxyphenylisopropylamine (3,4-methylenedioxyamphetamine). *J. Pharm Sci.* **1980**, *69*, 192−195.
(34) Onderwater, R. C.; Venhorst, J.; Commandeur, J. N. M.; Vermeulen, N. P. E. Design, synthesis, and characterization of 7-methoxy-4-(aminomethyl)coumarin as a novel and selective cytochrome P450 2D6 substrate suitable for high-throughput screening. *Chem. Res. Toxicol.* **1999**, *12*, 555−559.

(35) Omura, T.; Sato, R. The carbon monoxide-binding pigment of liver microsomes. II. Solubilization, purification, and properties. *J. Biol. Chem.* **1964**, *239*, 2379−2385.
(36) Jefcoate, C. R. Measurement of substrate and inhibitor binding to microsomal cytochrome P450 by optical-difference spectroscopy. *Methods Enzymol.* **1978**, *52*, 258−279.
(37) Hanna, I. H.; Krauser, J. A.; Cai, H.; Kim, M. S.; Guengerich, F. P. Diversity in mechanisms of substrate oxidation by cytochrome P450 2D6. Lack of an allosteric role of NADPH-cytochrome P450 reductase in catalytic regioselectivity. *J. Biol. Chem.* **2001**, *276*, 39553−39561.
(38) Solomon, I.; Bloembergen, N. Nuclear magnetic interactions in the HF molecule. *J. Chem. Phys.* **1956**, *25*, 261−266.
(39) Wester, M. R.; Johnson, E. F.; Marques-Soares, C.; Dansette, P. M.; Mansuy, D.; Stout, C. D. Structure of a substrate complex of mammalian cytochrome P450 2C5 at 2.3 A resolution: evidence for multiple substrate binding modes. *Biochemistry* **2003**, *42*, 6370−6379.
(40) Wester, M. R.; Johnson, E. F.; Marques-Soares, C.; Dijols, S.; Dansette, P. M.; Mansuy, D.; Stout, C. D. Structure of mammalian cytochrome P450 2C5 complexed with diclofenac at 2.1 A resolution: evidence for an induced fit model of substrate binding. *Biochemistry* **2003**, *42*, 9335−9345.
(41) Sali, A.; Blundell, T. L. Comparative protein modelling by satisfaction of spatial restraints. *J. Mol. Biol.* **1993**, *234*, 779−815.
(42) Laskowski, R. A.; Macarthur, M. W.; Moss, D. S.; Thornton, J. M. Procheck − a program to check the stereochemical quality of protein structures. *J. Appl. Crystallogr.* **1993**, *26*, 283−291.
(43) Colovos, C.; Yeates, T. O. Verification of protein structures − patterns of nonbonded atomic interactions. *Protein Sci.* **1993**, *2*, 1511−1519.
(44) Luthy, R.; Bowie, J. U.; Eisenberg, D. Assessment of protein models with 3-dimensional profiles. *Nature* **1992**, *356*, 83−85.
(45) Morris, G. M.; Goodsell, D. S.; Halliday, R. S.; Huey, R.; Hart, W. E.; Belew, R. K.; Olson, A. J. Automated docking using a Lamarckian genetic algorithm and an empirical binding free energy function. *J. Comput. Chem.* **1998**, *19*, 1639−1662.
(46) Rarey, M.; Kramer, B.; Lengauer, T.; Klebe, G. A fast flexible docking method using an incremental construction algorithm. *J. Mol. Biol.* **1996**, *261*, 470−489.
(47) Jones, G.; Willett, P.; Glen, R. C.; Leach, A. R.; Taylor, R. Development and validation of a genetic algorithm for flexible docking. *J. Mol. Biol.* **1997**, *267*, 727−748.
(48) Goodford, P. J. A computational procedure for determining energetically favorable binding sites on biologically important macromolecules. *J. Med. Chem.* **1985**, *28*, 849−857.
(49) Wang, R. X.; Liu, L.; Lai, L. H.; Tang, Y. Q. SCORE: A new empirical method for estimating the binding affinity of a protein−ligand complex. *J. Mol. Model.* **1998**, *4*, 379−394.
(50) Lindahl, E.; Hess, B.; van der Spoel, D. GROMACS 3.0: a package for molecular simulation and trajectory analysis. *J. Mol. Model.* **2001**, *7*, 306−317.
(51) Daura, X.; Mark, A. E.; van Gunsteren, W. F. Parametrization of aliphatic CHn united atoms of GROMOS96 force field. *J. Comput. Chem.* **1998**, *19*, 535−547.
(52) Scott, W. R. P.; Hunenberger, P. H.; Tironi, I. G.; Mark, A. E.; Billeter, S. R.; Fennen, J.; Torda, A. E.; Huber, T.; Kruger, P.; van Gunsteren, W. F. The GROMOS biomolecular simulation program package. *J. Phys. Chem. A* **1999**, *103*, 3596−3607.
(53) Hess, B.; Bekker, H.; Berendsen, H. J. C.; Fraaije, J. G. E. M. LINCS: A linear constraint solver for molecular simulations. *J. Comput. Chem.* **1997**, *18*, 1463−1472.
(54) Berendsen, H. J. C.; Postma, J. P. M.; van Gunsteren, W. F.; DiNola, A.; Haak, J. R. Molecular dynamics with coupling to an external bath. *J. Chem. Phys.* **1984**, *81*, 3684−3690.
(55) Meunier, B.; de Visser, S. P.; Shaik, S. Mechanism of oxidation reactions catalyzed by cytochrome p450 enzymes. *Chem. Rev.* **2004**, *104*, 3947−3980.

JM050338+